March 25, 2009
FERMILAB-CONF-09-088-E-PPD-T
arXiv:0903.4312

STATUS OF HIGGS BOSON SEARCHES AT THE TEVATRON

André Sopczak
Lancaster University
E-mail: andre.sopczak@cern.ch

ABSTRACT

Over the last years the Tevatron Run-II has extended several limits on Higgs boson masses and coupling which were pioneered during the LEP accelerator operation between 1989 and 2000. Higgs boson searches will also be at the forefront of research at the LHC. This review concisely discusses the experimental constraints set by the CDF and DØ collaborations in winter 2008/2009 at the beginning of the LHC era. Model-independent and model-dependent limits on Higgs boson masses and couplings have been set and interpretations are discussed both in the Standard Model and in extended models. Recently, for the first time the Tevatron excludes a SM Higgs boson mass range (160-170 GeV) beyond the LEP limit at 95% CL. The experimental sensitivities are estimated for the completion of the Tevatron programme.

Contribution to WONP'09 conference
Havana, Cuba, February 9-12

1 Introduction **1**

2 Production and Decay **1**

3 b-Quark Tagging **3**

4 Gluon Fusion $gg \to H \to WW$ **4**

5 Associated Production **4**
5.1 $WH(H \to b\bar{b})$ 4
5.2 $WH(H \to WW)$ 6
5.3 $ZH \to \ell\ell b\bar{b}$ 6
5.4 $ZH \to \nu\bar{\nu}b\bar{b}$ 6

6 $H \to \tau^+\tau^-$ **8**

7 $H \to \gamma\gamma$ **8**

8 $t\bar{t}H$ **9**

9 Combined SM Higgs Boson Limits **9**

10 Beyond the SM **11**
10.1 $b\bar{b}h$, $b\bar{b}H$, $b\bar{b}A$ 11
10.2 $h, H, A \to \tau^+\tau^-$ 12
10.3 H^+ 13
10.4 $H \to \gamma\gamma$ 15
10.5 H^{++} 15

11 Conclusions **16**

1. Introduction

The search for new particles is at the forefront of High Energy Physics. The discovery of a Higgs boson would shed light on electroweak symmetry breaking and the generation of mass in the Universe. Many searches for new particles were performed at LEP and stringent limits on Higgs bosons in the Standard Model (SM) and beyond were set. These limits are summarized in Table 1 (from [1]) including model-independent LEP limits and benchmark results in the Minimal Supersymmetric extension of the SM (MSSM) [2]. In addition to the limits from direct searches, some indication on the Higgs boson mass exist from precision electro-weak measurements, as shown in Fig. 1 (left and center plots from [3]). Up to about 4.2 fb^{-1} of data have been analyzed so far (winter 2008/9) by each Tevatron experiment, while about 5 fb^{-1} data have been recorded (about 6 fb^{-1} delivered). This report is structured similarly as Ref. [4] to allow to compare more directly the experimental progress from summer 2005 [4].

Both CDF and DØ have measured with precision various SM processes as illustrated in Fig. 1 (right plot from [5]). The figure includes also recent ZZ measurements [6, 7]. Figure 2 (from [8]) shows the delivered luminosity and its expectations.

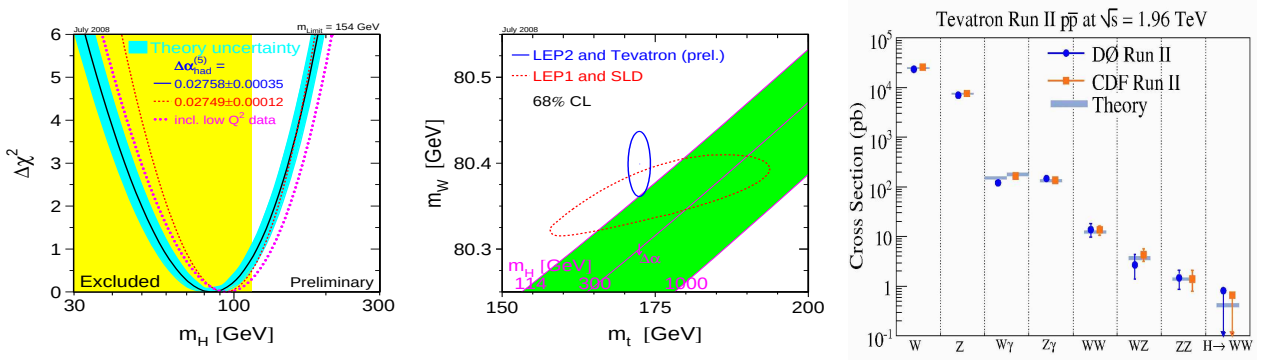

Figure 1. Left: Higgs boson mass prediction in the SM framework. The upper SM Higgs boson mass limit at 95% CL is 154 GeV. Center: smaller ellipse including LEP-2 and Tevatron data (solid line) prefers a region outside the SM Higgs boson mass band (m_H = 114 to 1000 GeV). The combined results from LEP-1 and SLD only are shown separately (dashed line). Right: overview of SM measurements by CDF and DØ, and indication of the expected cross-section for a 160 GeV SM Higgs boson.

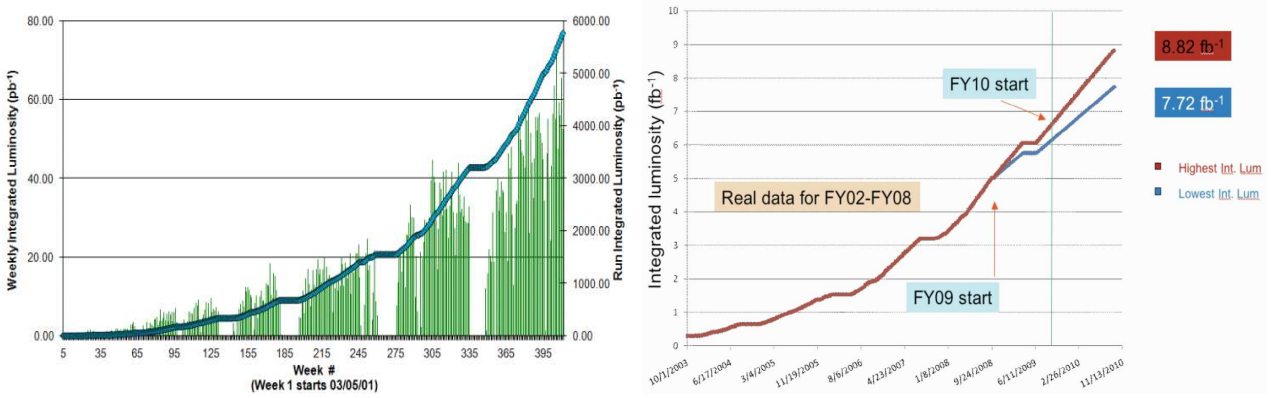

Figure 2. Left: integrated delivered Tevatron luminosity. Right: expectation for 2010 data-taking.

2. Production and Decay

The expected cross-section and branching ratios are shown in Fig. 3 (from [9] and [10]) as a function of the Higgs boson mass. It is interesting to note that corresponding to the current

collected data sample of about 5 fb^{-1} about 5000 SM Higgs bosons of 120 GeV could have already been produced in $\mathrm{p\bar{p}}$ collisions at each experiment. For a SM Higgs boson mass below about 200 GeV the decay width is below 1 GeV which is much below the detector resolution.

Table 1. Summary of Higgs boson mass limits at 95% CL. 'LEP' indicates a combination of the results from ALEPH, DELPHI, L3 and OPAL. If results from the experiments are not (yet) combined, examples which represent the different search areas from individual experiments are given. Details are given in Ref. [1].

Search	experiment	limit
Standard Model	LEP	$m_{\mathrm{H}}^{\mathrm{SM}} > 114.4$ GeV
Reduced rate and SM decay		$\xi^2 > 0.05 : m_{\mathrm{H}} > 85$ GeV
		$\xi^2 > 0.3 : m_{\mathrm{H}} > 110$ GeV
Reduced rate and $\mathrm{b\bar{b}}$ decay		$\xi^2 > 0.04 : m_{\mathrm{H}} > 80$ GeV
		$\xi^2 > 0.25 : m_{\mathrm{H}} > 110$ GeV
Reduced rate and $\tau^+\tau^-$ decay		$\xi^2 > 0.2 : m_{\mathrm{H}} > 113$ GeV
Reduced rate and hadronic decay		$\xi^2 = 1 : m_{\mathrm{H}} > 112.9$ GeV
		$\xi^2 > 0.3 : m_{\mathrm{H}} > 97$ GeV
	ALEPH	$\xi^2 > 0.04 : m_{\mathrm{H}} \approx 90$ GeV
Anomalous couplings	L3	d, d_{B}, Δg_1^{Z}, $\Delta\kappa_\gamma$ exclusions
MSSM (no scalar top mixing)	LEP	almost entirely excluded
General MSSM scan	DELPHI	$m_{\mathrm{h}} > 87$ GeV, $m_{\mathrm{A}} > 90$ GeV
Larger top-quark mass	LEP	strongly reduced $\tan\beta$ limits
MSSM with CP-violating phases	LEP	strongly reduced mass limits
Visible/invisible Higgs decays	DELPHI	$m_{\mathrm{H}} > 111.8$ GeV
Majoron model (max. mixing)		$m_{\mathrm{H,S}} > 112.1$ GeV
Two-doublet Higgs model	DELPHI	$\mathrm{hA} \to \mathrm{bbbb} : m_{\mathrm{h}} + m_{\mathrm{A}} > 150$ GeV
(for $\sigma_{\max}$)		$\tau^+\tau^-\tau^+\tau^- : m_{\mathrm{h}} + m_{\mathrm{A}} > 160$ GeV
		$(\mathrm{AA})\mathrm{A} \to 6\mathrm{b} : m_{\mathrm{h}} + m_{\mathrm{A}} > 150$ GeV
		$(\mathrm{AA})\mathrm{Z} \to 4\mathrm{b\ Z} : m_{\mathrm{h}} > 90$ GeV
		$\mathrm{hA} \to \mathrm{q\bar{q}q\bar{q}} : m_{\mathrm{h}} + m_{\mathrm{A}} > 110$ GeV
Two-doublet model scan	OPAL	$\tan\beta > 1 : m_{\mathrm{h}} \approx m_{\mathrm{A}} > 85$ GeV
Yukawa process	DELPHI	$C > 40 : m_{\mathrm{h,A}} > 40$ GeV
Singly-charged Higgs bosons	LEP	$m_{\mathrm{H}^\pm} > 78.6$ GeV
$\mathrm{W}^\pm\mathrm{A}$ decay mode	DELPHI	$m_{\mathrm{H}^\pm} > 76.7$ GeV
Doubly-charged Higgs bosons	DELPHI/OPAL	$m_{\mathrm{H}^{++}} > 99$ GeV
$\mathrm{e^+e^-} \to \mathrm{e^+e^-}$	L3	$h_{\mathrm{ee}} > 0.5 : m_{\mathrm{H}^{++}} > 700$ GeV
Fermiophobic $\mathrm{H} \to \mathrm{WW}, \mathrm{ZZ}, \gamma\gamma$	L3	$m_{\mathrm{H}} > 108.3$ GeV
$\mathrm{H} \to \gamma\gamma$	LEP	$m_{\mathrm{H}} > 109.7$ GeV
Uniform and stealthy scenarios	OPAL	depending on model parameters

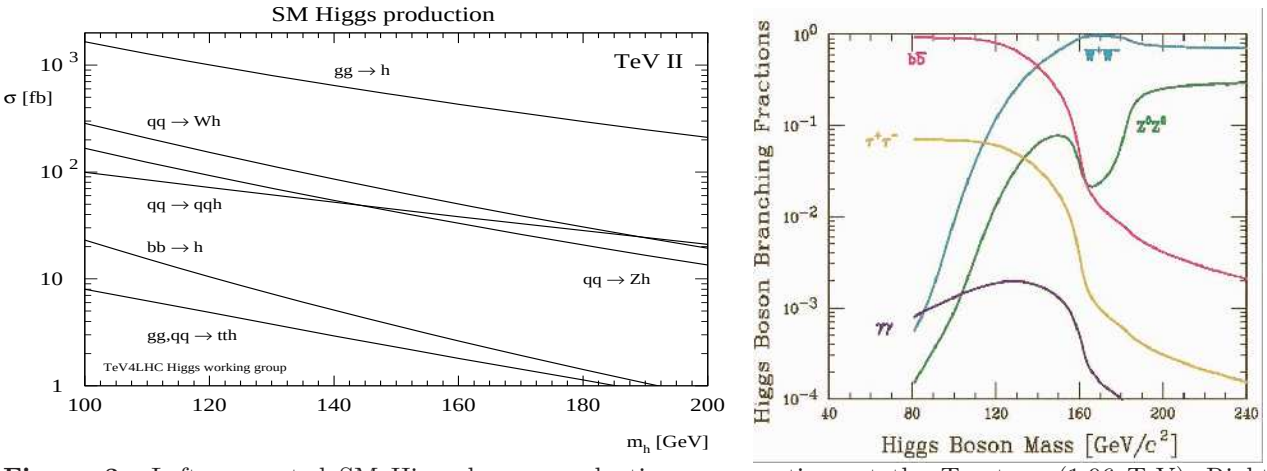

Figure 3. Left: expected SM Higgs boson production cross-sections at the Tevatron (1.96 TeV). Right: expected Higgs boson decay branching ratios for a SM Higgs boson masses. At the Tevatron, $\mathrm{b\bar{b}}$ and WW decays are dominant, in addition the $\tau^+\tau^-$ decay mode has a significant contribution.

3. b-Quark Tagging

The b-tagging capabilities are most important for the low-mass Higgs boson searches and a critical parameter is the impact parameter resolution of the vertex detector. The improvement of the impact parameter resolution with a sensitive layer very close to the interaction point is illustrated in Fig. 4 (left plot from [11] and center plot from [12]). In CDF this layer is called L00 and in DØ it is called L0. These innermost layers contribute significantly to the b-tagging performance. Figure 4 (right plot from [13]) shows also the DØ b-quark tagging performance including L0. An example of a quadruply b-tagged event is shown in Fig. 5 (from [14]).

Efficient B hadron tagging has already been demonstrated in data with $Z \to b\bar{b}$ events. These measurements contribute to the energy resolution and energy scale determinations. Figure 6 (left plot from [15], center plot from [16] and right plot from [17]) shows the reconstruction of the $Z \to b\bar{b}$ mass and the good agreement between data and simulation for b-tagged events.

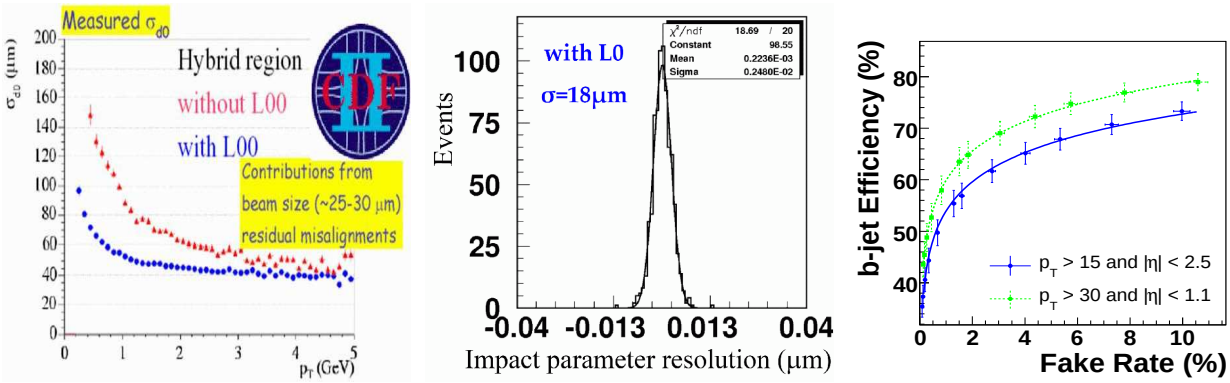

Figure 4. Left: CDF impact parameter resolution as a function of p_T for tracks traversing passive material in vertex detector, with (blue dots) and without (red triangles) use of L00 hits. Center: DØ impact parameter resolution after the installation of a new vertex detector layer (L0), which improved the resolution by 40%. Right: DØ b-quark tagging performance for $Z \to b\bar{b}$ and $Z \to q\bar{q}$ events. The error bars include statistical and systematic uncertainties.

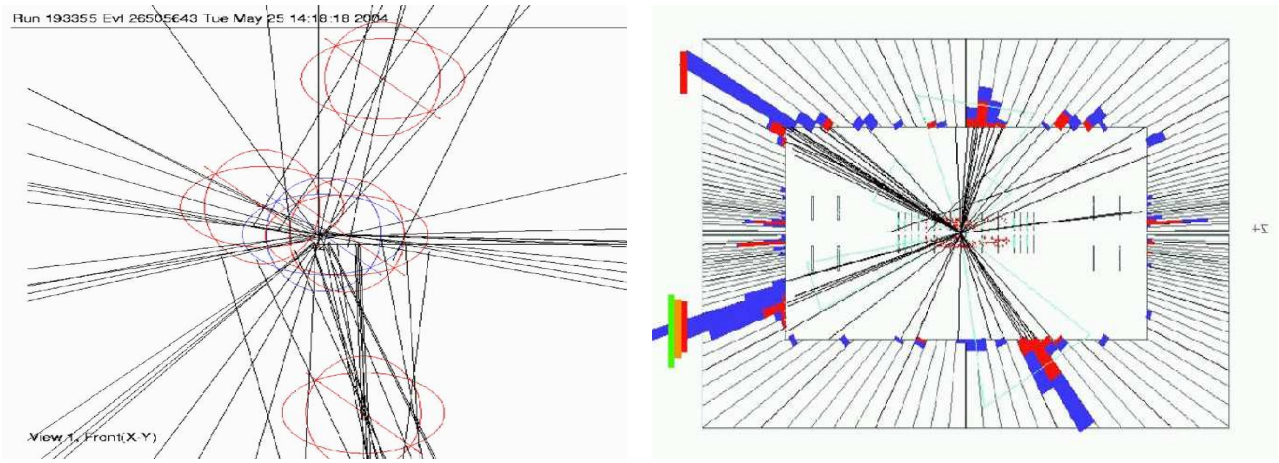

Figure 5. DØ example of b-tagged event. Left: reconstructed tracks near the interaction point. Right: jets clearly visible in the calorimeter.

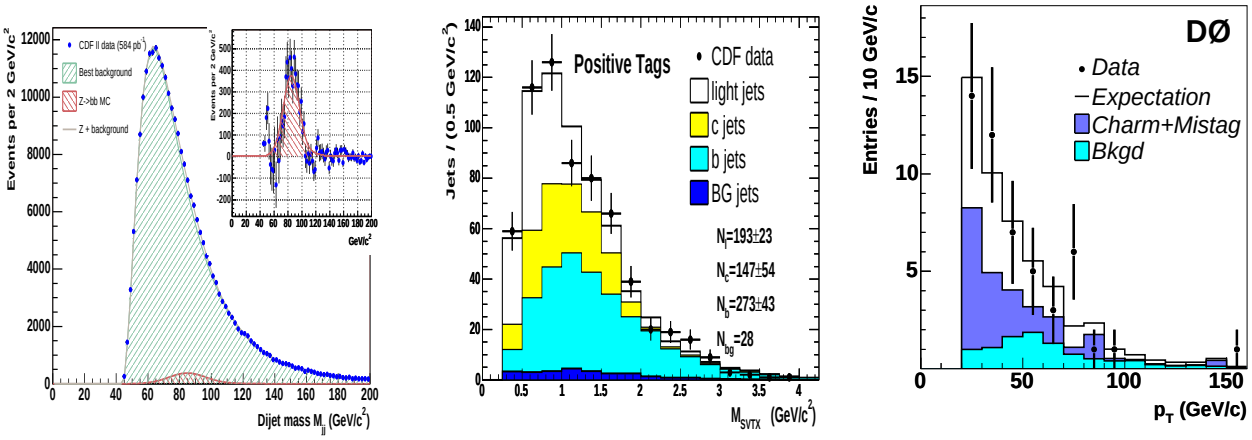

Figure 6. Left: CDF $Z \to b\bar{b}$ signal extracted in double-b-tagged data, relevant for $H \to b\bar{b}$ searches. Center: CDF invariant mass of tracks at the secondary vertex for positively tagged jets. Right: DØ P_t distribution for b-tagged jets of Z+jets events.

4. Gluon Fusion $gg \to H \to WW$

For Higgs boson masses above about 135 GeV the process $gg \to H \to WW$ becomes important. The production and decay process is illustrated in Fig. 7, also shown is a background process leading to the same final state particles. The spin information allows separation of signal and background. The angle between the opposite charged leptons $\Delta\Phi_{ll}$ tends to be smaller for the signal than for the background as shown in Fig. 7 (from [18]). Based on 3.0-4.2 fb^{-1} total luminosity the neural network output for $gg \to H \to WW$ process and limits are shown in Fig. 8 (from [18]) and based on 3.6 fb^{-1} in Fig. 9 (from [19]). Owing to the overwhelming $b\bar{b}$ background, the $gg \to H(H \to b\bar{b})$ channel is not feasible at the Tevatron.

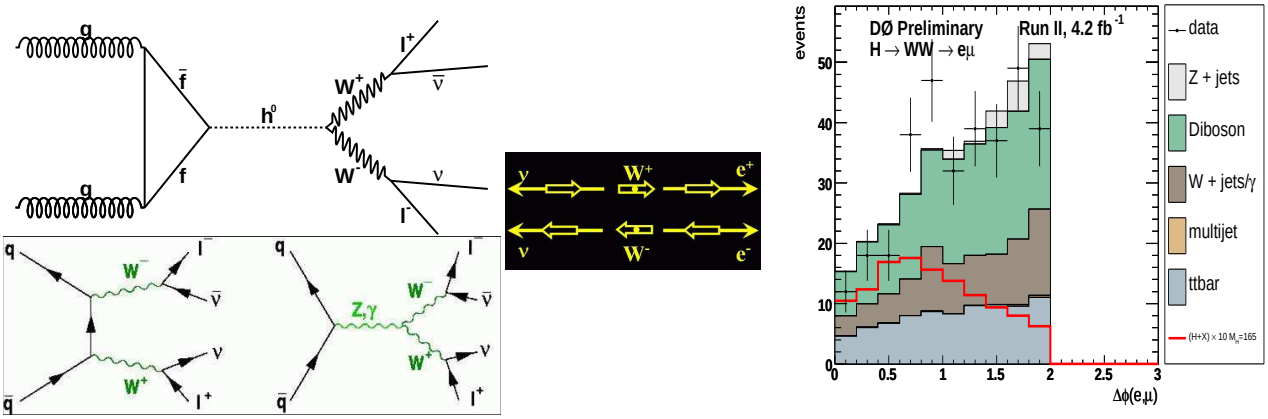

Figure 7. Left: $gg \to H(H \to WW)$ signal and background processes. Center: indication of spin correlations between final state leptons and W pairs, which lead to different dilepton azimuthal angular ($\Delta\Phi_{ll}$) distributions for signal and background. Right: DØ $\Delta\Phi_{ll}$ distribution for data, and simulated signal and background. $\Delta\Phi_{ll}$ is predicted to be smaller for the signal.

5. Associated Production

5.1. $WH(H \to b\bar{b})$

An important discovery channel is the reaction $WH(H \to b\bar{b})$, where the W decays either to $e\nu$ or $\mu\nu$. The tagging of two b-quarks improves the signal to background ratio as shown in Fig. 10 (from [20]) and Fig. 11 (from [21]).

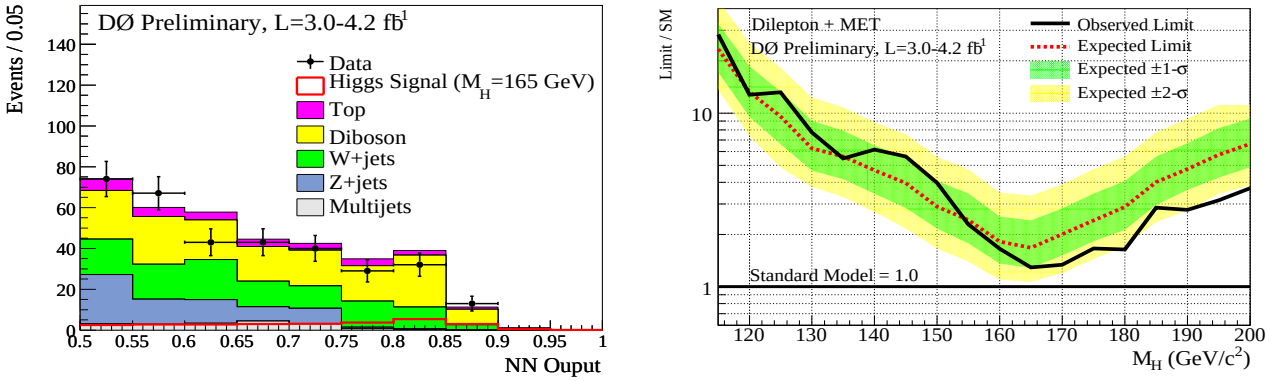

Figure 8. DØ gg → H(H → WW). Left: Neural network output. Right: limit at 95% CL.

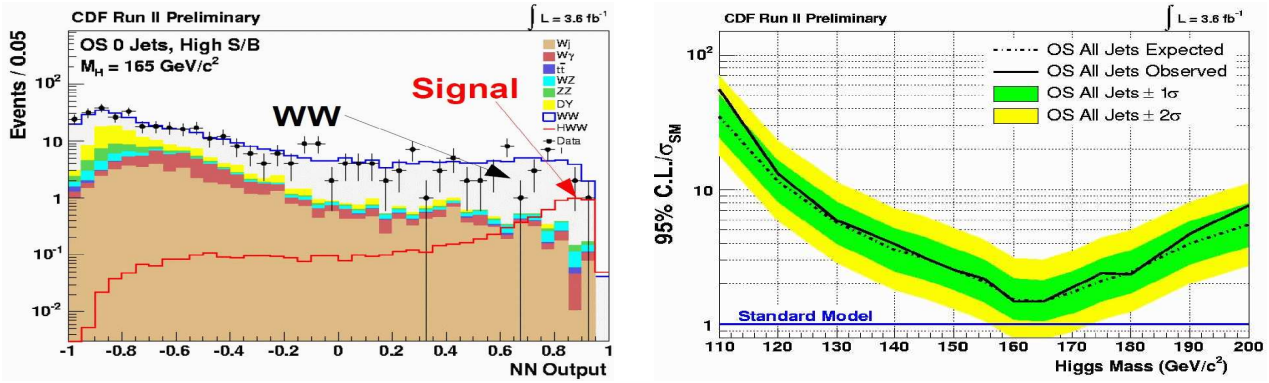

Figure 9. CDF gg → H(H → WW). Left: Neural network output. Right: limit at 95% CL.

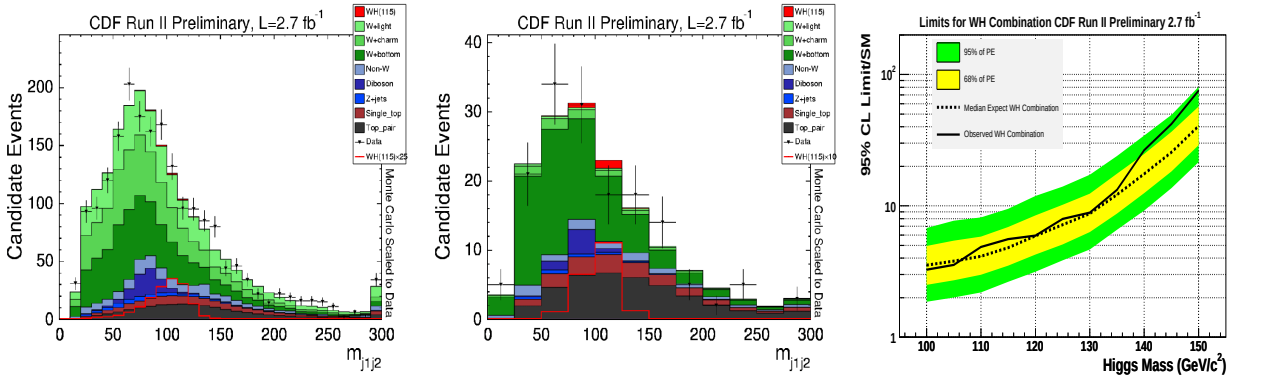

Figure 10. CDF WH(H → $b\bar{b}$). Matrix Element and Boosted Decision Tree Techniques (ME+BDT). Left: single b-tagging. Center: double b-tagging. Right: limit at 95% CL from combined ME+BDT and neural network analysis results.

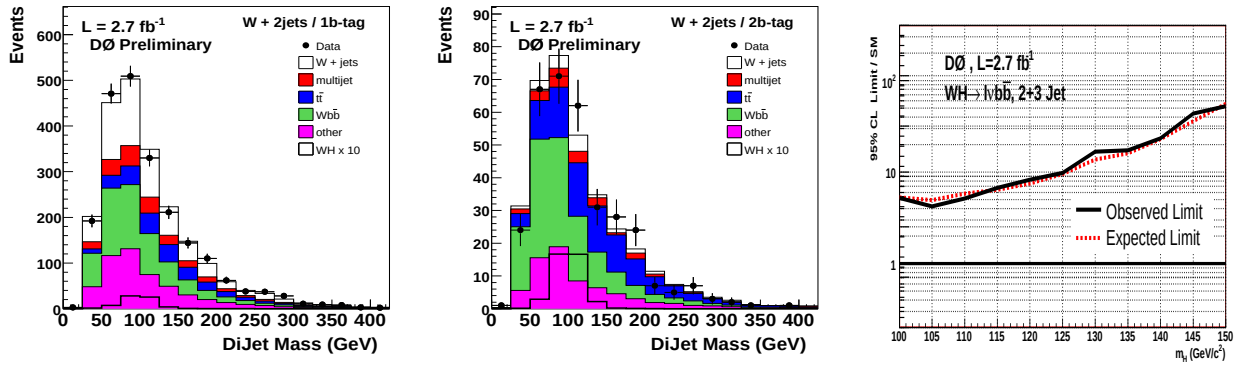

Figure 11. DØ WH(H → $b\bar{b}$). Left: single b-tagging. Center: double b-tagging. Right: limit at 95% CL.

5.2. WH(H → WW)

Recent results for the search WH(H → WW) in the like-signed charged lepton final state are shown in Fig. 12 (from [22], 2.7 fb^{-1} luminosity) and Fig. 13 (from [23], 3.6 fb^{-1} luminosity), which lead to weaker sensitivity as in the H → b$\bar{\text{b}}$ decay mode.

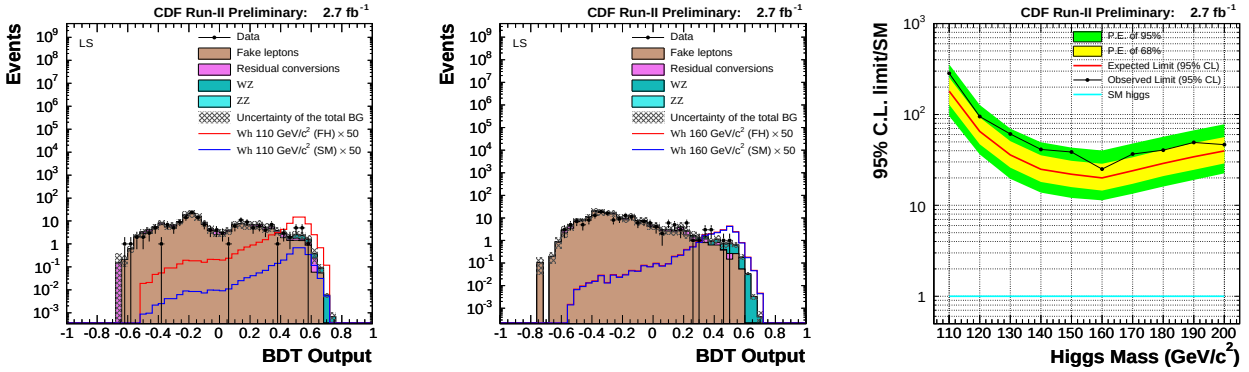

Figure 12. CDF WH(H → WW). Left: comparison of simulated background and observed number of events (110 GeV Higgs boson selection) for the Boosted Decision Tree (BDT) output. Center: comparison of simulated background and observed number of events (160 GeV Higgs boson selection). Right: limit at 95% CL.

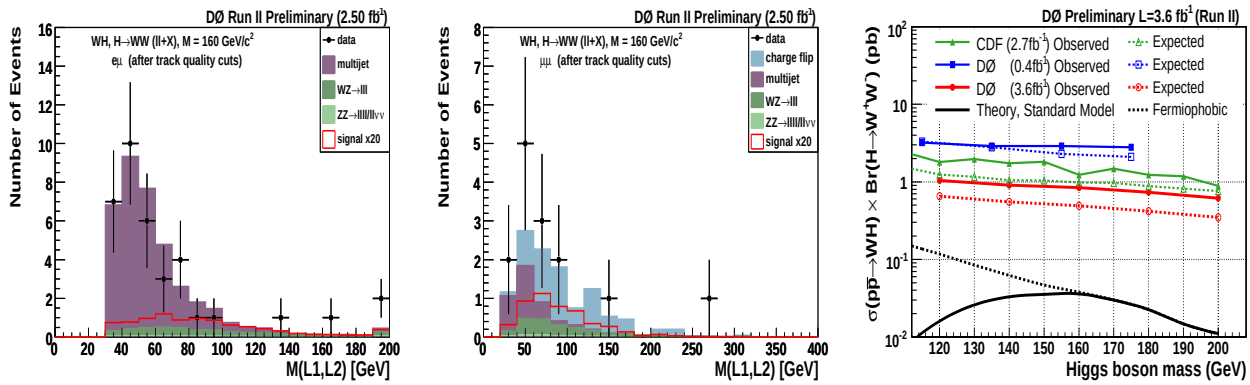

Figure 13. DØ WH(H → WW). Left: eμ invariant mass. Center: $\mu\mu$ invariant mass. Right: limit at 95% CL.

5.3. ZH → $\ell\ell$b$\bar{\text{b}}$

The CDF and DØ collaborations have searched for ZH → e$^+$e$^-$b$\bar{\text{b}}$ and $\mu^+\mu^-$b$\bar{\text{b}}$ signals. These signals are very clean, however, they have a small production cross-section. The results are shown in Fig. 14 (from [24]) and Fig. 15 (from [25]).

5.4. ZH → $\nu\bar{\nu}$b$\bar{\text{b}}$

Both Tevatron collaborations have searched for a ZH → $\nu\bar{\nu}$b$\bar{\text{b}}$ signal. The results from the expected missing energy and b-jet signal are shown in Fig. 16 (from [26]) and Fig. 17 (from [27]).

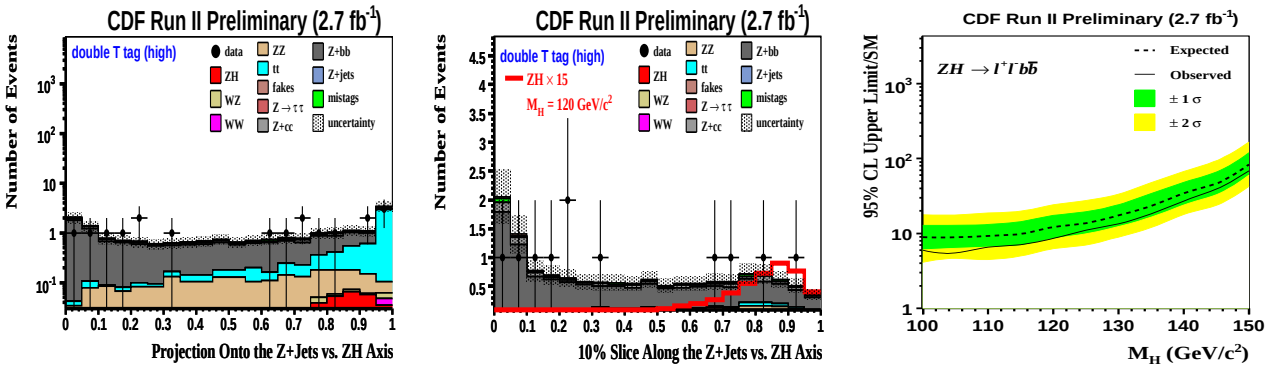

Figure 14. CDF ZH($Z \to \ell\ell$)($H \to b\bar{b}$). Left: $Z \to \ell^+\ell^-$ neural network output (2-dimensional) projection. Mostly Z+jets and $t\bar{t}$ background. Center: $Z \to \ell^+\ell^-$ neural network output (2-dimensional) projection. Right: limit at 95% CL.

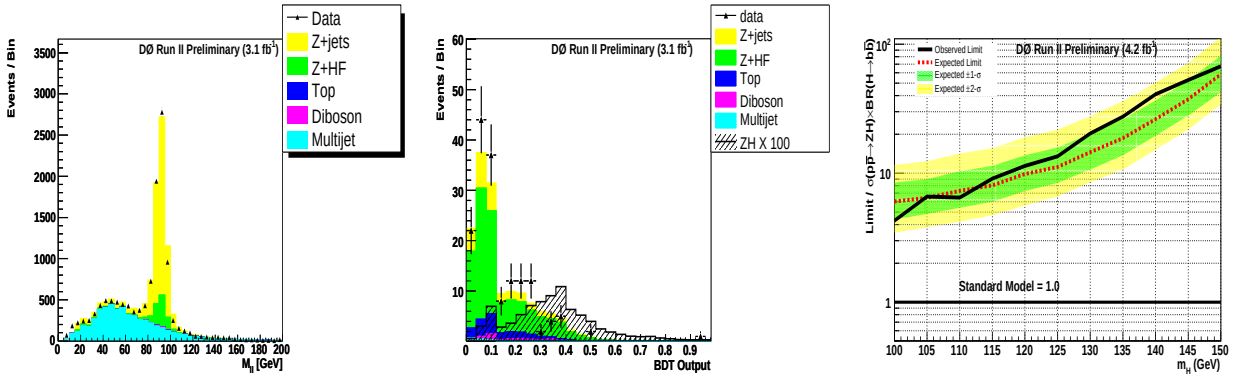

Figure 15. DØ ZH ($Z \to \ell\ell$)($H \to b\bar{b}$). Left: $Z \to e^+e^-$ invariant mass. Center: $Z \to \mu^+\mu^-$ boosted decision tree (BDT) output. Right: cross-section limit combined with previous $Z \to \ell\ell$ results.

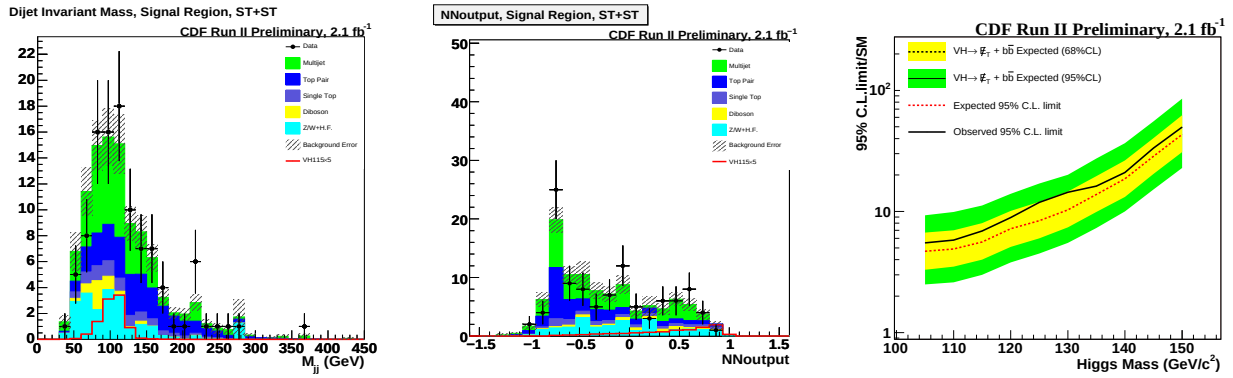

Figure 16. CDF ZH($Z \to \nu\nu$)($H \to b\bar{b}$). Left: invariant di-jet mass. Center: neural network. Right: limit at 95% CL.

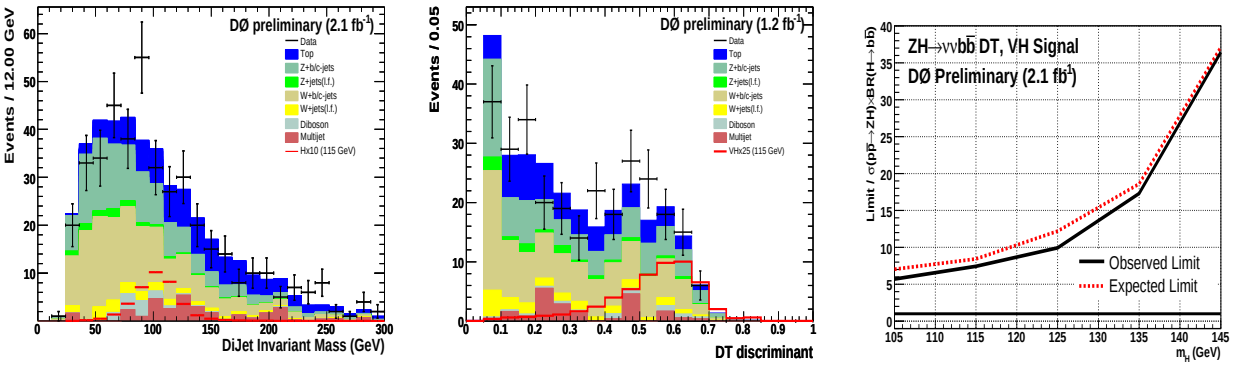

Figure 17. DØ ZH($Z \to \nu\nu$)($H \to b\bar{b}$). Left: invariant di-jet mass. Center: discriminant variable output. Right: limit at 95% CL.

6. $H \to \tau^+\tau^-$

Both Tevatron collaborations have searched for a $H \to \tau^+\tau^-$ signal. Results are shown in Figs. 18 (from [28]) and 19 (from [29]).

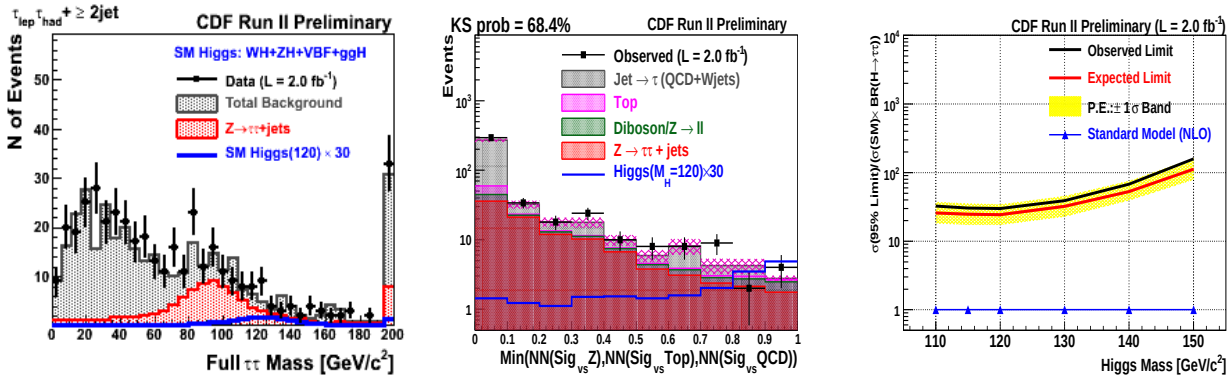

Figure 18. CDF ($H \to \tau^+\tau^-$). Left: invariant mass. Center: neural network output. Right: limit at 95% CL.

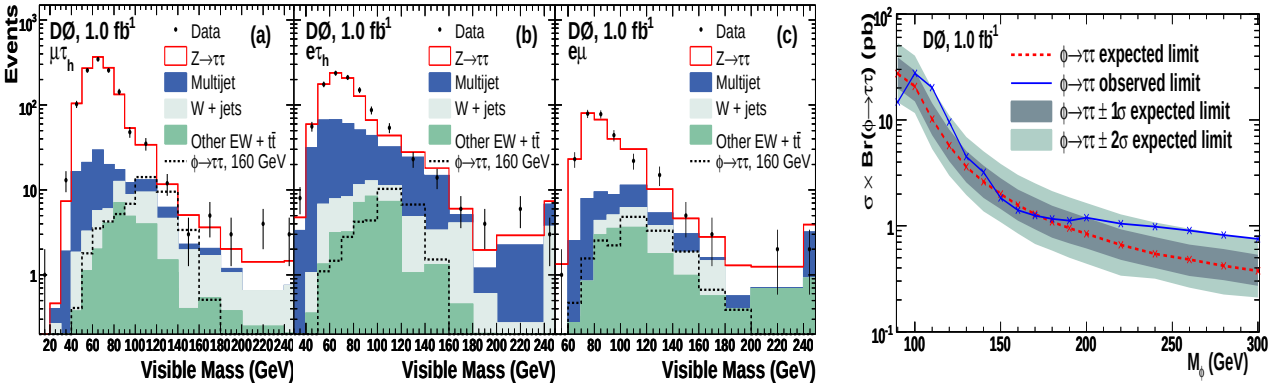

Figure 19. DØ ($H \to \tau^+\tau^-$). Left: invariant masses for $\mu\tau_h$, $e\tau_h$ and $e\mu$. Right: limit at 95% CL.

7. $H \to \gamma\gamma$

Both Tevatron collaborations have searched for a $H \to \gamma\gamma$ signal. Results are shown in Figs. 20 (from [30]) and 21 (from [31]).

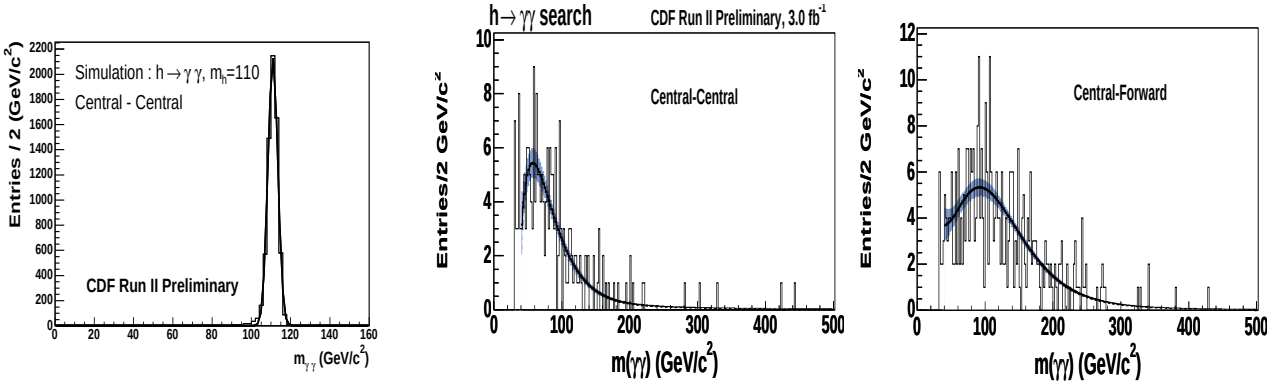

Figure 20. CDF ($H \to \gamma\gamma$). Left: simulated $H \to \gamma\gamma$ invariant mass. Center: invariant mass spectrum with both photons in the central region. Right: invariant mass spectrum with one photon in the central region and one in the forward region.

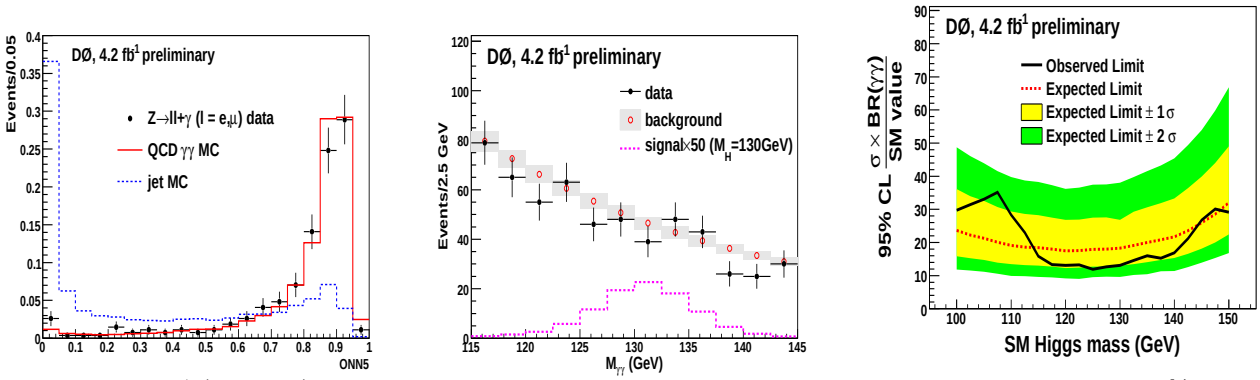

Figure 21. DØ ($H \to \gamma\gamma$). Left: neural network output. Center: invariant mass. Right: limit at 95% CL.

8. $t\bar{t}H$

Both Tevatron collaborations have searched for a $t\bar{t} \to t\bar{t}H$ signal. Results are shown in Figs. 22 (from [32]) and 23 (from [33]).

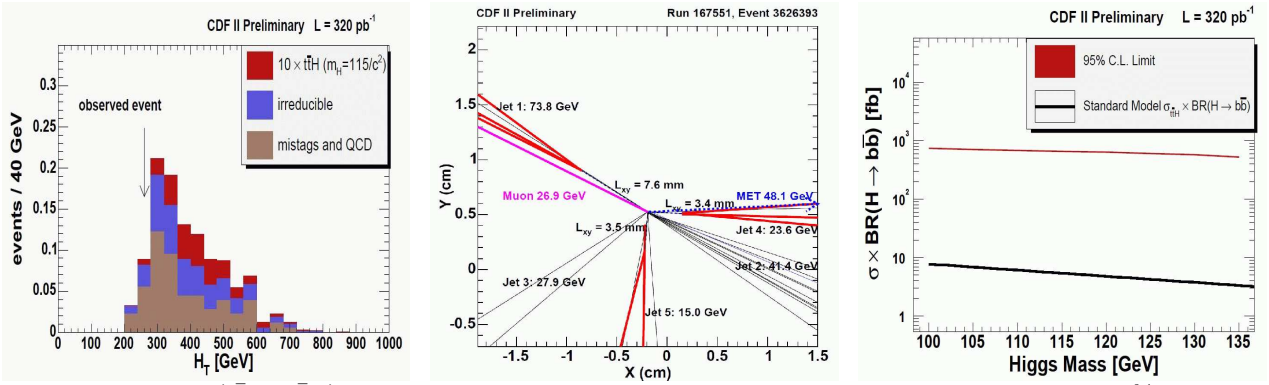

Figure 22. CDF ($t\bar{t} \to t\bar{t}H$). Left: H_T distribution. Center: candidate event. Right: limit at 95% CL.

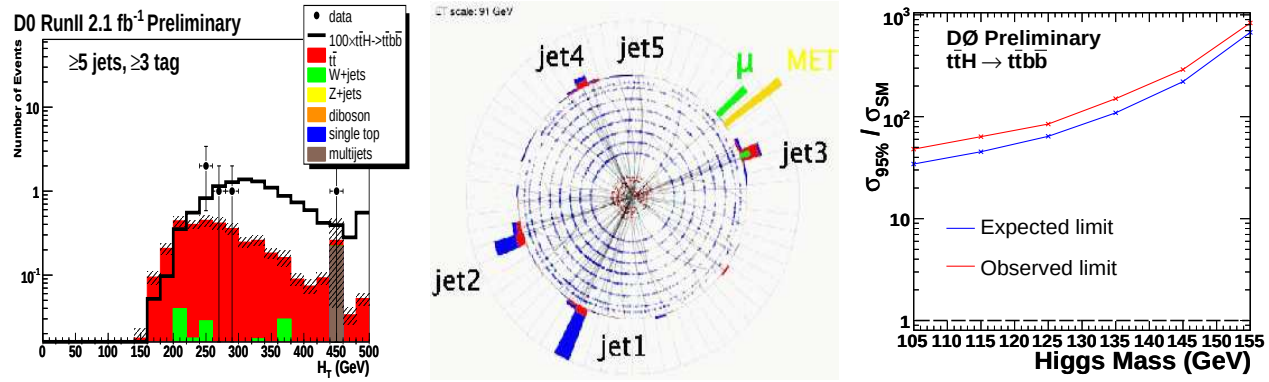

Figure 23. DØ ($t\bar{t} \to t\bar{t}H$). Left: H_T distribution. Center: candidate event. Right: limit at 95% CL.

9. Combined SM Higgs Boson Limits

The large progress in sensitivity increase between results from summer 2005 (left plot from [4]) and recent combined CDF and DØ results (right plot from [34]) are shown in Fig. 24 with up to 4.2 fb^{-1}. The achieved sensitivity in the various search channels is summarized in Table 2.

Improvements will continue to come from optimized b-quark tagging, and also from larger e/μ acceptance, better jet mass resolution, and from using advanced analysis techniques. Higher Higgs boson sensitivities will also result from the increase in luminosity. Currently (winter 2008/9) about 5 fb^{-1} are recorded per experiment, and the total delivered luminosity will increase up to about 8.5 fb^{-1} (6.8 fb^{-1} recorded) as illustrated in Fig. 2. Resulting sensitivity estimates are shown in Fig. 25 (from [35]).

Table 2. Summary of observed and expected limits (where available) as factor compated to the SM expectation at 95% CL from CDF and DØ. The note numbers refer to CDF and DØ notes, respectively.

Channel	experiment	m_{H} (GeV)	$\mathcal{L}$ (fb^{-1})	limit factor obs.	limit factor exp.	Reference note
$\mathrm{H}\to\mathrm{WW}\to\ell\nu\ell\nu$	CDF	160	3.6	1.5	1.5	9500 [19]
	DØ	160	4.2	1.7	1.8	5871 [18]
$\mathrm{WH}\to\mathrm{l}\nu\mathrm{b}\bar{\mathrm{b}}$	CDF	115	2.7	5.6	4.8	9596 [20]
	DØ	115	2.7	6.7	6.4	5828 [21]
$\mathrm{WH}\to\mathrm{WWW}$	CDF	160	2.7	25	20	7307 [22]
	DØ	160	3.6	10	18	5873 [23]
$\mathrm{ZH}\to\ell\ell\mathrm{b}\bar{\mathrm{b}}$	CDF	115	2.7	7.1	9.9	9665 [24]
	DØ	115	4.2	9.1	8.0	5876 [25]
$\mathrm{ZH}\to\nu\bar{\nu}\mathrm{b}\bar{\mathrm{b}}$	CDF	115	2.1	6.9	5.6	9642 [26]
	DØ	115	2.1	7.5	8.4	5586 [27]
W/ZH, VBF, ggH	CDF	115	2.0	31	25	9248 [28]
$(H\to\tau^+\tau^-)$	DØ	115	1.0	27	28	5883 [29]
$\mathrm{H}\to\gamma\gamma$	CDF	–	3.0	–	–	9586 [30]
	DØ	115	4.2	16	19	5858 [31]
$\mathrm{t}\bar{\mathrm{t}}\mathrm{H}$	CDF	–	0.3	–	–	9508 [32]
	DØ	115	2.1	64	45	5739 [33]

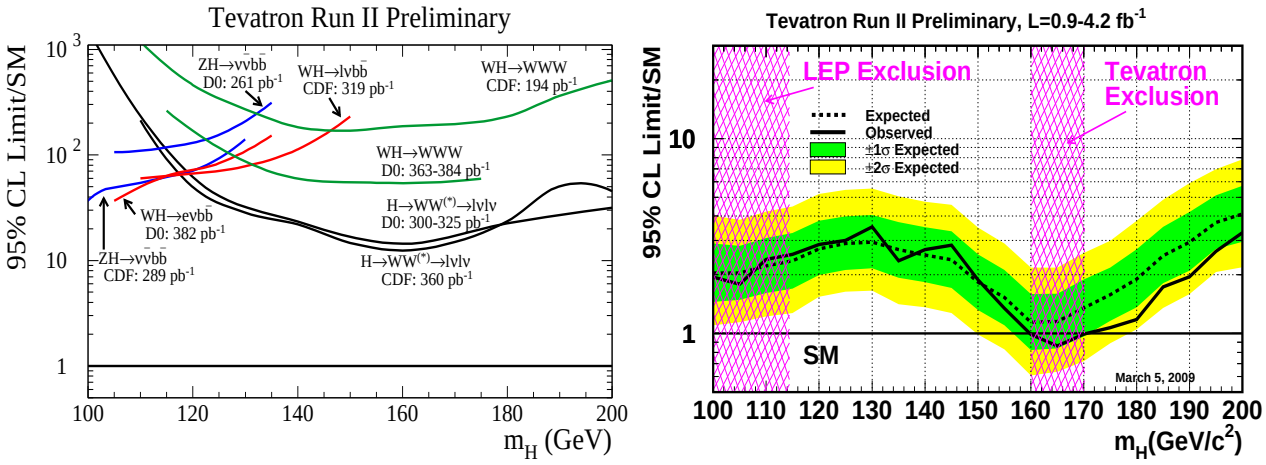

Figure 24. Comparison of progress between summer 2005 and winter 2008/9. Left: ratio of observed cross-section limit and expected SM cross-section, status summer 2005. Right: current combined CDF and DØ limits at 95% CL. Status winter 2008/9: Note that a region between 160 and 170 GeV mass is excluded.

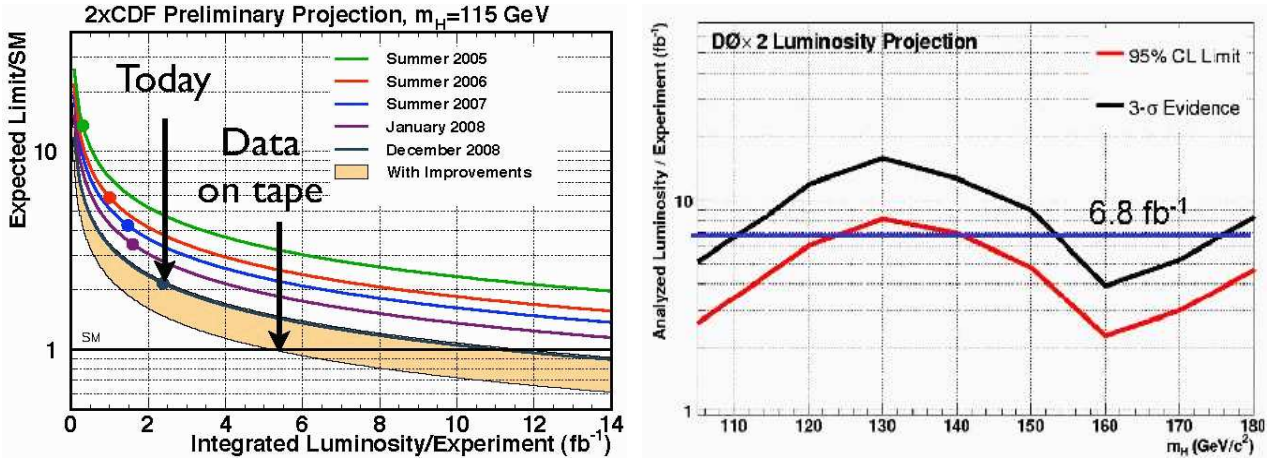

Figure 25. Outlook. Left: for a 115 GeV Higgs boson. Right: for a mass range between 105 to 180 GeV.

10. Beyond the SM

10.1. $b\bar{b}h$, $b\bar{b}H$, $b\bar{b}A$

Higgs boson production processes in association with b-quarks in $p\bar{p}$ collisions have been calculated in two ways: in the five-flavor scheme [36], where only one b-quark has to be present in the final state, while in the four-flavor scheme [37], two b-quarks are explicitly required in the calculation. Both calculations are available at next-to-leading order (NLO QCD), and agree taking into account the theoretical uncertainties. Figure 26 (from [38]) illustrates these processes for h production at leading order (LO), and analogous diagrams can be drawn for the H and A bosons. The cross-section depends on $\tan^2\beta$ and on other Supersymmetric parameters as given by $\sigma \times BR_{\rm SUSY} \approx 2\sigma_{\rm SM} \tan^2\beta/(1+\delta_b)^2 \times 9/(9+(1+\delta_b)^2)$, where $\delta_b = k \tan\beta$ with k depending on the SUSY parameters, in particular also on A_t, the mixing in the scalar top sector, the gluino mass, the μ parameter, stop and sbottom masses. The dependence of the production cross-section enhancement factor on $\tan\beta$ is shown in Fig. 26 (right plot from [38]). At tree-level the production cross-section rises with $\tan^2\beta$.

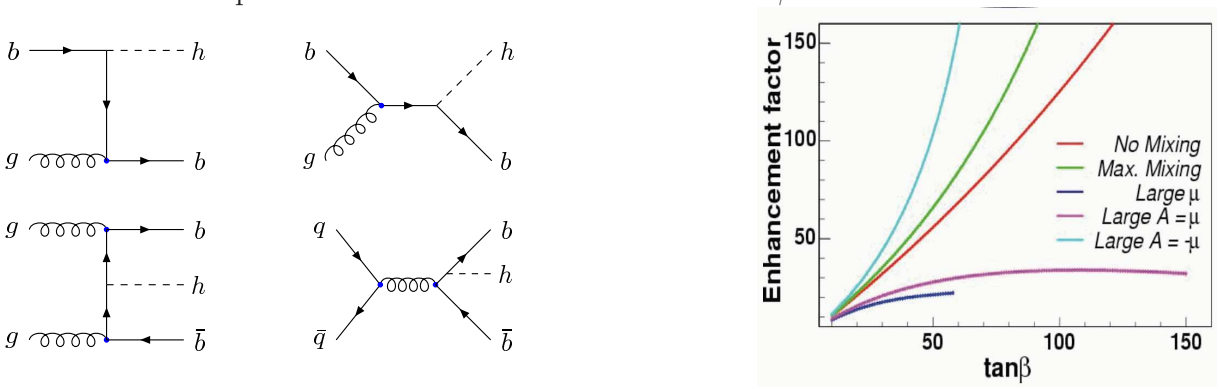

Figure 26. DØ. Left: leading-order Feynman diagrams for neutral Higgs boson production in the five-flavor scheme (top) and four-flavor scheme (bottom). Right: enhancement factor as a function of $\tan\beta$.

There is no indication of a $b\bar{b}A$ production in the data. Results from CDF and DØ are shown in Fig. 27 (from [39]) and Fig. 28 (from [40]). In the CDF results based on 1.9 fb^{-1} data statistical and systematic errors contribute about equally, therefore, with about 8 fb^{-1} data, cross-section sensitivities could be improved by about 20%, thus $\tan\beta$ sensitivities by about 10%. Estimates reported in 2005 [4] were too optimistic.

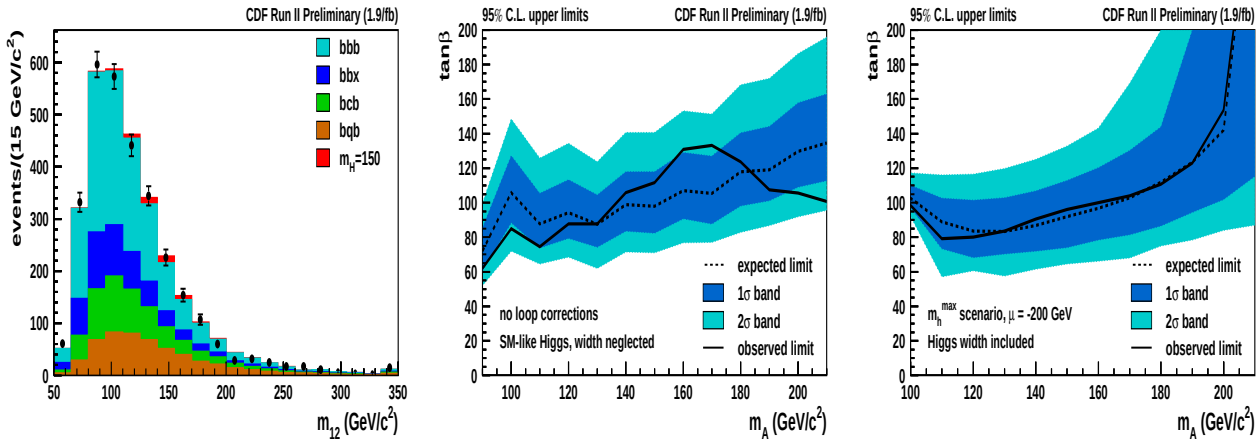

Figure 27. CDF. $b\bar{b}A(A \to b\bar{b})$. Left: invariant mass of the two most energetic jets $m_A = 150$ GeV. Center: limits on $\tan\beta$ in the gereral Two Higgs Doublet Model (THDM). Right: limits on $\tan\beta$ in the MSSM for the mhmax scenario.

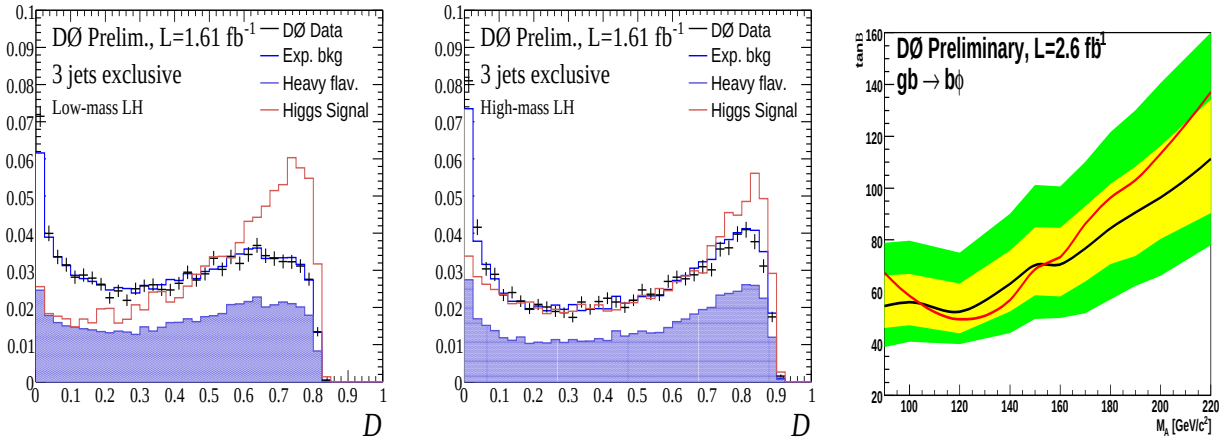

Figure 28. DØ. $b\bar{b}A(A \to b\bar{b})$. Left: discriminant variable output, low-mass. Center: discriminant variable output, high-mass. Right: limit at 95% CL.

10.2. $h, H, A \to \tau^+\tau^-$

The signature for $h, H, A \to \tau^+\tau^-$ opens additional possibilities for a Higgs boson discovery. Results from CDF and DØ are shown in Fig. 29 (from [41]) and Fig. 30 (from [42]).

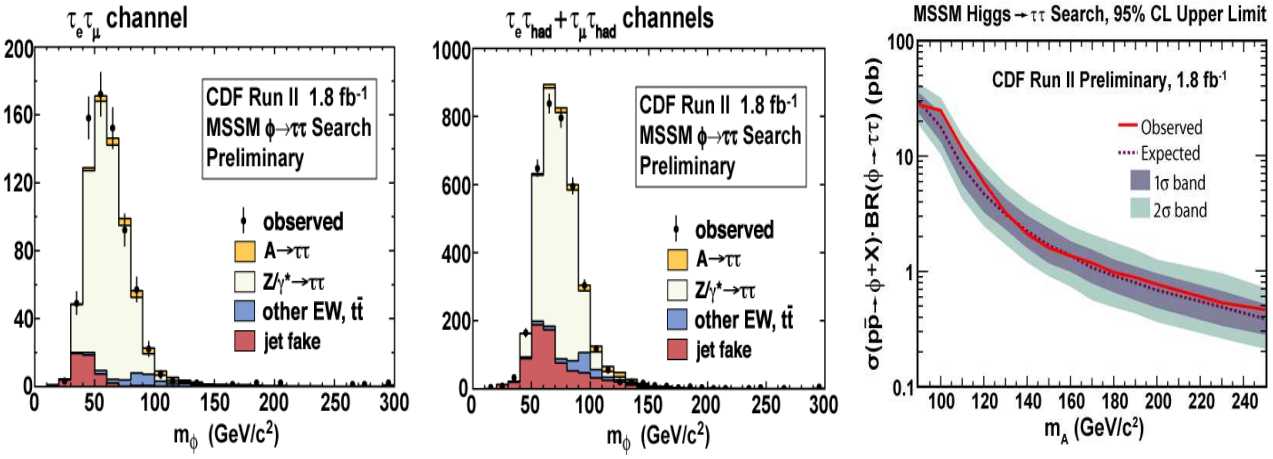

Figure 29. CDF. Left: invariant mass eμ channel for $\Phi = A$ with $m_A = 140$ GeV. Center: invariant mass $\ell\tau_h$ channel where ℓ represents an electron or a muon. Right: cross-section limit at 95% CL.

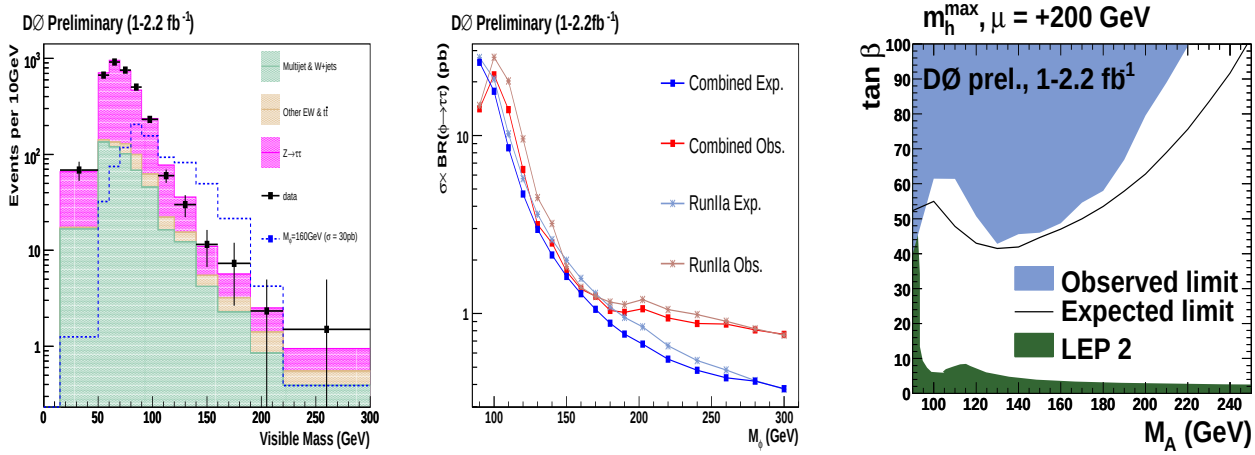

Figure 30. DØ. Left: visible mass for $\Phi = A$ with $m_A = 160$ GeV. Center: cross-section limit at 95% CL. Right: MSSM limit at 95% CL.

10.3. H^+

The decay of top quarks $t \to H^+b$ is possible in general Higgs boson models with two Higgs boson doublets. The expected top and charged Higgs boson branching fractions are shown in Fig. 31 (left plot from [43]) as a function of $\tan\beta$ for a specific MSSM parameter set. The expected SM top decay rate would be modified. No deviation from the SM top decay rates is observed. Results from CDF for 0.192 fb^{-1} are shown in Fig. 31 (right plot from [44]) and from DØ for 1 fb^{-1} are shown in Figs. 32 and 33 (from [43]).

An independent search has been carried out by DØ based on measuring the ratio $R = \sigma(t\bar{t})_{\ell+\text{jets}}/\sigma(t\bar{t})_{\ell^+\ell^-}$ [45]. In the SM $R = 1$, while a decay $t \to H^+b$ changes this ratio. Results are summarized in Fig. 34 (from [45]) for a leptofobic charged Higgs boson.

A recent charged Higgs boson search by CDF focuses on the reaction $t \to H^+b$ ($H^+ \to c\bar{s}$) [46] based on 2.2 fb^{-1} data. The hadronic charged Higgs boson decay mode would allow a precise H^+ mass reconstruction. Results are summarized in Fig. 35 (from [46]).

In the high mass regime ($m_{H^+} > m_t$) the search for charged Higgs bosons has been performed similar as for the single top s-channel analysis with $\mathcal{L} = 0.9$ fb^{-1}. The reaction is $q\bar{q}' \to H^+ \to t\bar{b} \to W^+b\bar{b} \to \ell^+\nu b\bar{b}$ [47], where ℓ represents an electron or a muon. Results are summarized in Fig. 36 (from [47]).

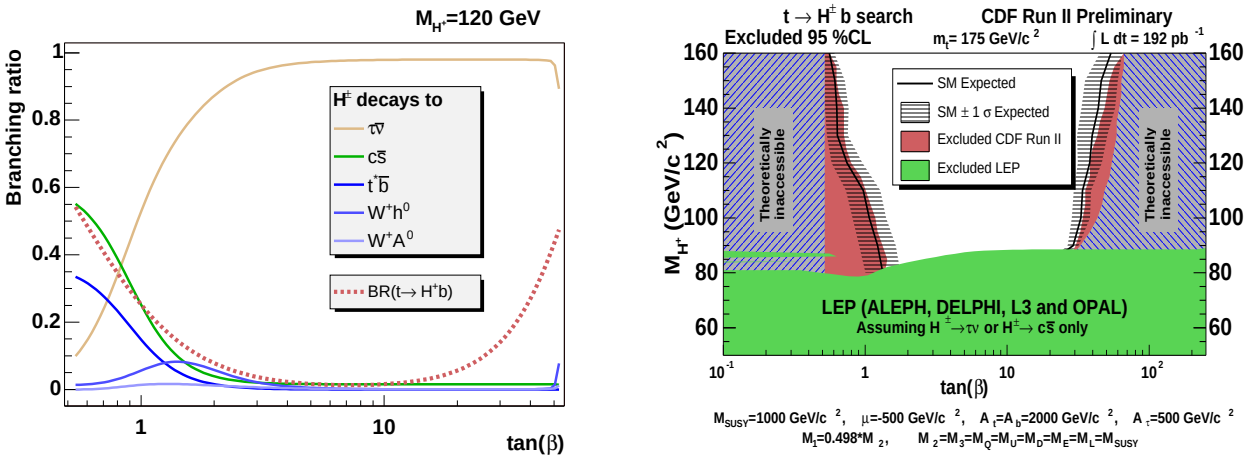

Figure 31. Left: branching ratios for a 120 GeV charged Higgs boson production in top decays and charged Higgs boson decays as a function of $\tan\beta$ in the MSSM. Right: CDF. Limits on the charged Higgs boson mass as function of $\tan\beta$ for a specific set of MSSM parameters.

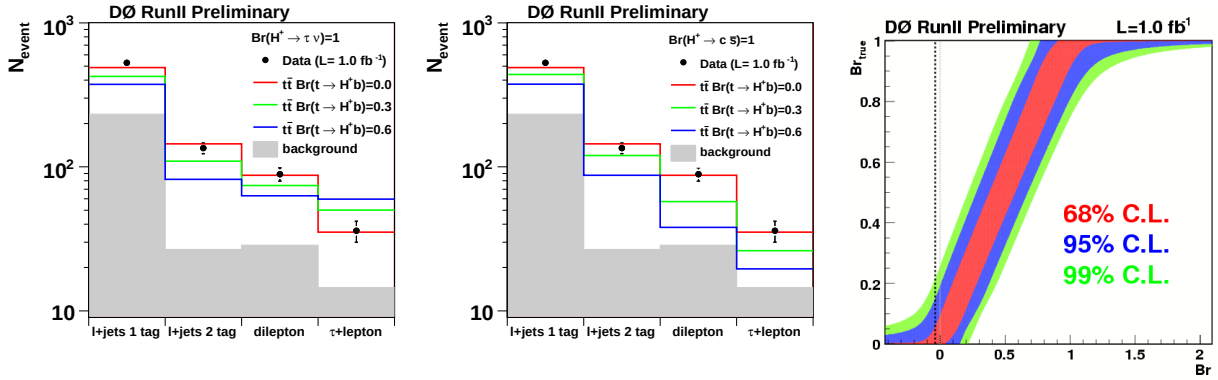

Figure 32. DØ. Left: variation of number of expected events for $t \to H^+b$ ($H^+ \to \tau^+\nu$). Center: variation of number of expected events for $t \to H^+b$ ($H^+ \to cs$). Right: BR($t \to H^+b$) limits and type II THDM leading order calculation expectation.

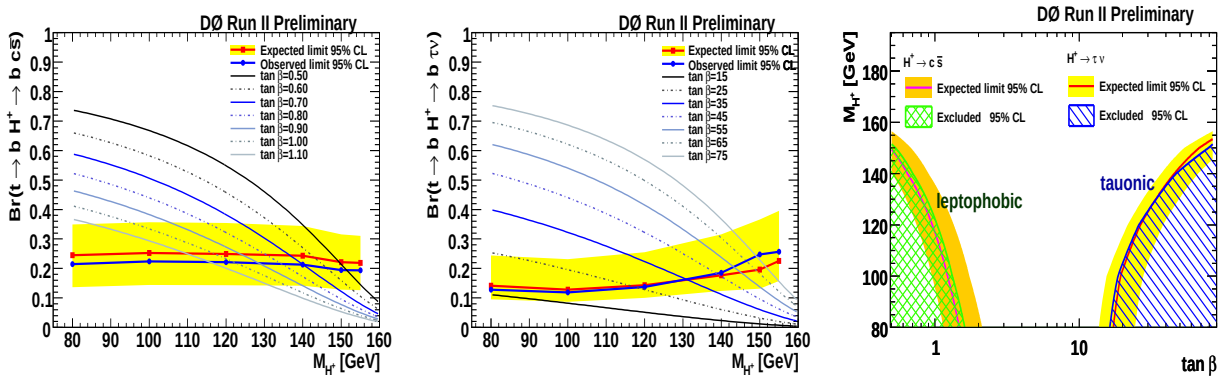

Figure 33. DØ. Left: BR(t → H⁺b)(H⁺ → cs) limit at 95% CL. Center: BR(t → H⁺b)($H^+ \to \tau^+\nu$) limit at 95% CL. Right: limits on the charged Higgs boson mass as function of tan β for a specific set of MSSM parameters.

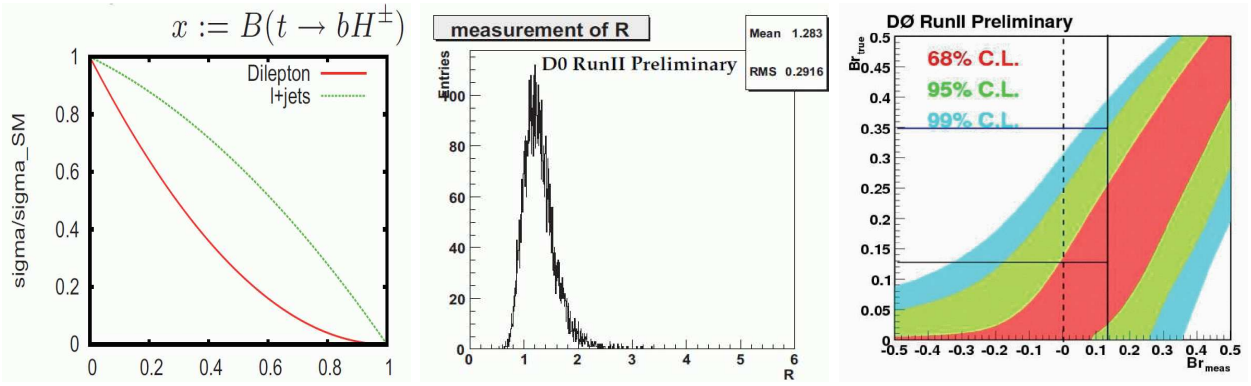

Figure 34. DØ. Left: modified cross-sections relative to the SM cross-section as functions of BR(t → H⁺b). Center: cross-section ratio, R, distribution generated from the 10,000 pseudo-experiments. Right: Feldman-Cousins confidence interval bands as functions of measured and generated branching fraction BR(t → H⁺b). For a leptophobic 80 GeV charged Higgs boson, BR(H⁺ → cs)=1, BR(t → H⁺b) limits at 95% CL are 0.35 (observed, solid line) and 0.25 (expected, dotted line).

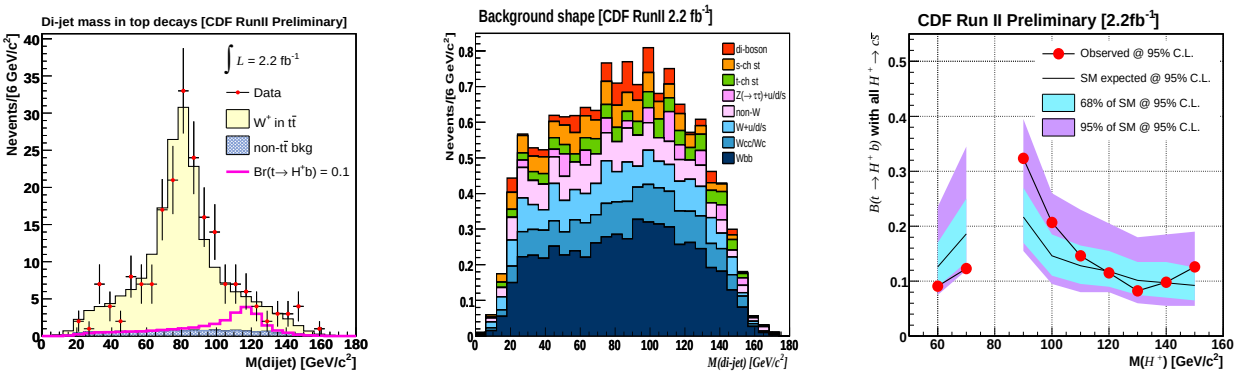

Figure 35. CDF. Left: di-jet mass in top decays. Center: background contributions to the di-jet mass in top decays. Right: model-independent BR(t → H⁺b) limit for BR(H⁺ → $c\bar{s}$) = 1. In order to cover any generic anomalous charged Higgs boson, the search is extended below the W mass.

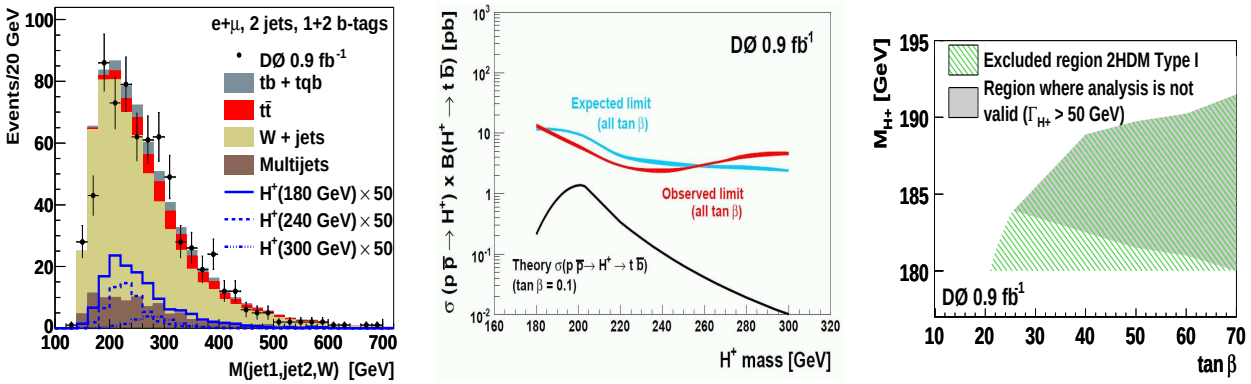

Figure 36. DØ. $p\bar{p} \to H^+ \to t\bar{b}$. Left: invariant charged Higgs boson mass (type III model). Center: cross-section limit in THDM (type II). Right: THDM excluded regions for model type I.

10.4. H $\to \gamma\gamma$

In fermiophobic Higgs boson models, the dominant decay mode could be H $\to \gamma\gamma$. The Higgs boson could be produced in the associated production with a vector boson and vector boson fusion (VBF) production mechanisms. No indication of such reactions have been observed and limits are set as shown in Fig. 37 from CDF (left plot [30]) and from DØ (center and right plots [48]).

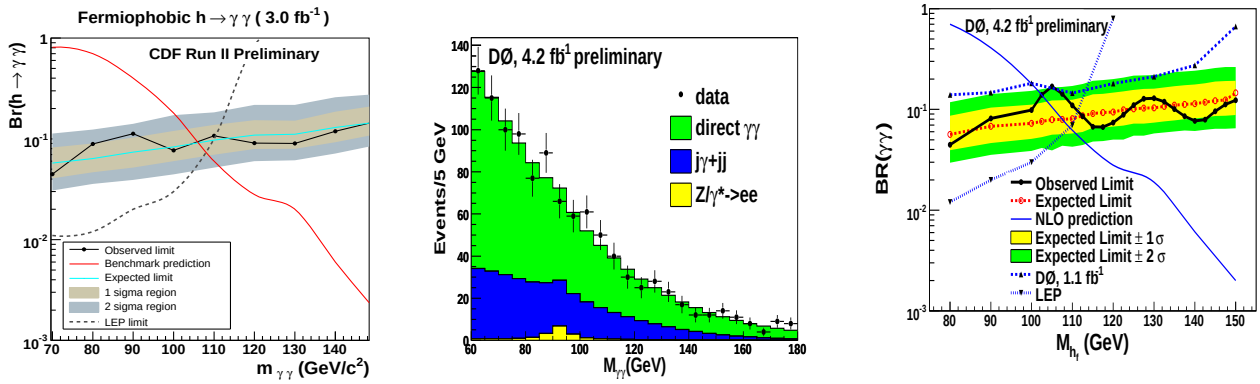

Figure 37. Fermiophobic Higgs. H $\to \gamma\gamma$. Left: CDF limits at 95% CL with $\mathcal{L} = 3.0$ fb^{-1}. Center: DØ invariant $\gamma\gamma$ mass distribution with $\mathcal{L} = 4.2$ fb^{-1}. Right: DØ limits at 95% CL with $\mathcal{L} = 4.2$ fb^{-1}.

10.5. H^{++}

The possibility of doubly-charged Higgs boson exists in models with Higgs boson triplets. Pairs of like-sign charged leptons are expected from the decay of the doubly-charged Higgs bosons. No indication has been observed in the data. The di-muon mass spectrum and limits on the doubly-charged Higgs boson mass are shown in Fig. 38 from CDF (left plot [49]) and from DØ (center and right plots) [50]).

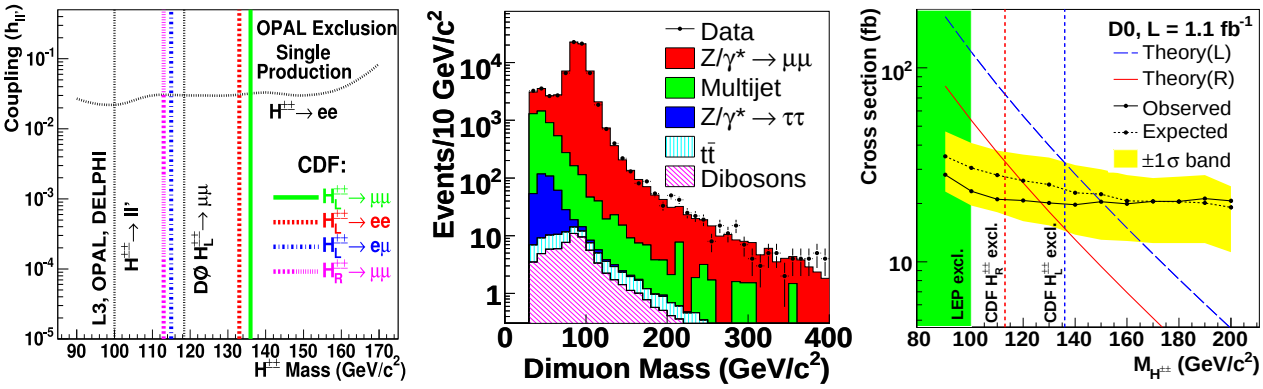

Figure 38. Left: CDF doubly-charged Higgs boson mass limits at 95% CL. Center: DØ di-muon mass spectrum. Right: DØ doubly-charged Higgs boson mass limits at 95% CL.

11. Conclusions

Much has been learned from the searches for Higgs bosons at LEP. The Tevatron Run-II searches for Higgs bosons are well under way and already have set several limits exceeding some previous LEP limits. For the SM Higgs boson, searches for gluon fusion with WW decays, associated production WH with $b\bar{b}$ and WW decays, and ZH $\to \nu\nu b\bar{b}$ decays have been performed previously. Updates of these searches have been reported and compared to a previous report [4] with results from summer 2005. More recently, searches for the SM reactions ZH $\to \ell\ell b\bar{b}$, H $\to \gamma\gamma$ and $t\bar{t} \to t\bar{t}H$ have been performed in addition. Beyond the Standard Model, the searches at the Tevatron for $b\bar{b}A$, H^+, H^{++}, h $\to \gamma\gamma$ and $\tau^+\tau^-$ have led to new limits on couplings and masses. The close collaboration of phenomenologists and experimentalists is crucial to fully exploit the potential of the collected data. The sensitivity of the SM Higgs searches is evolving rapidly, significantly faster than the increase in sensitivity from improved statistics alone. The first direct SM exclusion beyond the LEP results was achieved at high mass, around 170 GeV, in summer 2008. Incorporating the ongoing improvements, by the end of 2010 running, exclusion over virtually the full mass range favoured by the electroweak fits is achievable. In addition three sigma evidence will be possible over much of the same range.

Acknowledgments

I would like to thank my colleagues from the CDF and DØ Higgs working groups for discussions and comments on the manuscript, in particular Peter Bussey, Craig Group, Matthew Herndon, Thomas Wright and Un-ki Yang from the CDF Collaboration, Gavin Davies, Sebastien Greder, Phillip Gutierrez and Alex Melnitchouk from the DØ Collaboration, and Oscar Stål from the phenomenology group at Uppsala University.

References

[1] A. Sopczak, Proceedings QFTHEP'04, St. Petersburg, Russia; and WONP'05, Havana, Cuba, hep-ph/0502002, and references therein.

[2] A. Sopczak, "MSSM Higgs boson searches at LEP", Talk at the 13th International Conference on Supersymmetry and Unification of Fundamental Interactions (SUSY'05), Durham, UK, July 18-23, 2005, hep-ph/0602136.

[3] The LEP Electroweak Working Group, http://lepewwg.web.cern.ch/LEPEWWG/.

[4] A. Sopczak, hep-ph/0605236. FERMILAB-CONF-06-134-E-T, May 2006. Presented at Aspen Summer Workshop on Collider Physics: from the Tevatron to the LHC to the Linear Collider, Aspen, Colorado, 15 August - 11 September, 2005.

[5] CDF and DØ Collaborations, summary of SM cross-section measurements.

[6] T. Aaltonen et al., CDF Collaboration, Phys. Rev. Lett. **100**, 201801 (2008).

[7] V. M. Abazov et al., DØ Collaboration, Phys. Rev. Lett. **101**, 171803 (2008).

[8] Fermilab Operations, http://www-bdnew.fnal.gov/operations/lum/lum.html.

[9] F. Maltoni et al. in TeV4LHC Workshop, Fermilab, Chicago, October 2005. hep-ph/0612172.

[10] A. Djouadi, J. Kalinowski and M. Spira, Comput. Phys. Commun. **108**, 56 (1998).

[11] C. S. Hill, CDF Collaboration, Nucl. Instrum. Meth. **A 530**, 1 (2004).

[12] DØ Collaboration, R. Lipton, private communications (2009).

[13] I. Iashvili in TeV4LHC Workshop, Fermilab, Chicago, October 2005. hep-ph/0612172, and updated plot.

[14] A. Haas, "A Search for Neutral Higgs Bosons at High $\tan\beta$ in Multi-jet Events from $p\bar{p}$ Collisions at $\sqrt(s) = 1960$ GeV", University of Washington, PhD Thesis (2005).

[15] J. Donini et al., Nucl. Instrum. Meth. **A 596**, 354 (2008).

[16] T. Altonen et al., CDF Collaboration, arXiv:0812.4458, submitted to Phys. Rev. D.

[17] V. M. Abazov et al., DØ Collaboration, Phys. Rev. Lett. **94**, 161801 (2005).

[18] DØ Collaboration, DØ note 5871, March 6, 2009.

[19] CDF Collaboration, CDF note 9500, July 25, 2008, and update Moriond'09.

[20] CDF Collaboration, CDF note 9463 (ME+BDT analysis), August 8, 2008; CDF note 9468 (NN analysis), August 1, 2008; and CDF note 9596 (combined ME+BDT and NN limit), November 19, 2008.

[21] DØ Collaboration, DØ note 5828, February 5, 2009.

[22] CDF Collaboration, CDF note 7307, December 19, 2008.

[23] DØ Collaboration, DØ note 5873, March 13, 2009.

[24] CDF Collaboration, CDF note 9665, December 11, 2008.

[25] DØ Collaboration, DØ note 5876, March 12, 2009.

[26] CDF Collaboration, CDF note 9642, July 11, 2008 and public web page December 29, 2008.

[27] DØ Collaboration, DØ note 5586, February 29, 2008.

[28] CDF Collaboration, CDF note 9248, February 22, 2008.

[29] DØ Collaboration, DØ note 5883, March 9, 2009.

[30] CDF Collaboration, CDF note 9586, October 29, 2008.

[31] DØ Collaboration, DØ note 5858, February 24, 2009.

[32] S. Lai, "Search for Standard Model Higgs Boson Produced in Association with a Top-Antitop Quark Pair in 1.96 TeV Proton-Antiproton Collisions", University of Toronto, PhD Thesis (2006), CDF note 9508; A. Anastassov et al. CDF and D0 Collaborations, AIP Conf. Proc. **903**, 73 (2007).

[33] DØ Collaboration, DØ note 5739, July 28, 2008.

[34] CDF and DØ Collaborations, CDF note 9713, DØ note 5889, March 12, 2009.

[35] CDF and DØ Collaborations, "Projections", http://www-cdf.fnal.gov/physics/new/hdg/results/.

[36] J. Campbell, R. K. Ellis, F. Maltoni and S. Willenbrock, Phys. Rev. **D 67**, 095002 (2003).

[37] S. Dawson, C. B. Jackson, L. Reina and D. Wackeroth, Phys. Rev. **D 69**, 074027 (2004); S. Dittmaier, M. Krämer and M. Spira, Phys. Rev. **D 70**, 074010 (2004).

[38] V. M. Abazov et al., DØ Collaboration, Phys. Rev. Lett. **95**, 151801 (2005).

[39] CDF Collaboration, CDF note 9284, April 7, 2008.

[40] DØ Collaboration, DØ note 5726, July 25, 2008.

[41] CDF Collaboration, CDF note 9071, October 22, 2007.

[42] DØ Collaboration, DØ note 5728, July 25, 2008, and note 5740, July 29, 2008.

[43] DØ Collaboration, DØ note 5715, July 25, 2008.
[44] A. Abulencia et al., The CDF Collaboration, Phys. Rev. Lett. **96**, 042003 (2006).
[45] V. Abazov, DØ Collaboration, Phys. Rev. Lett. **100**, 192003 (2008);
DØ note 5371, March 13, 2007; DØ note 5466, August 14, 2008.
[46] CDF Collaboration, CDF note 9322, August 1, 2008.
[47] DØ Collaboration, submitted Phys. Rev. Lett. (2008). arXiv:0807.0859; and cross-section limit released to Summer Conferences 2008.
[48] DØ Collaboration, DØ note 5880, March 11, 2009.
[49] D. Acosta et al., CDF Collaboration, Phys. Rev. Lett. **95**, 071801 (2005).
[50] V.M. Abazov et al., DØ Collaboration, Phys. Rev. Lett. **101**, 071803 (2008).